2D periodic patterns and transition to turbulence in active nematics

Author: Irina Pi Jaumà*
Facultat de Física, Universitat de Barcelona, Diagonal 645, 08028 Barcelona.

Advisor: Jaume Casademunt Viader
(Dated: January 16, 2019)

Abstract: We explore and characterize the 2D stationary patterns emerging from the spontaneous flow instability of an active nematic fluid, solving numerically the dynamics for a minimal model that has been proposed as the paradigm of active turbulence. We find that such solutions exist in the range of activity parameter $150 < |\mathcal{Z}| < 1500$. We also test numerically the long-wavelength instability of such states, showing that they are unstable to period-doubling perturbations for activity above 500, leading to apparently chaotic dynamics. This confirms a scenario of transition to turbulence that has been proposed in this system, and reinforces the idea that the proposed minimal model, which neglects flow alignment coupling and assumes absence of topological defects, does capture the universal features of active turbulence.

I. INTRODUCTION

The term active matter refers to nonequilibrium condensed systems composed of self-driven units (called active particles), each capable of converting stored or ambient free energy into movement [1]. Living matter provides the most obvious examples of active systems, from the cytoskeleton of living cells or bacterial suspensions to fish schools or bird flocks. Active particles are usually elongated and exhibit a privileged direction, and the interaction among each other gives rise to collective motion with nonequilibrium properties, such as pattern formation, order-disorder transitions and turbulence.

The type of active matter that we will focus on are "active gels" [2, 3], which consist of a one-component fluid with a local orientation nematic order parameter, either polar or apolar. In the polar case the local orientation is defined by a polarization vector $\mathbf{p}$, while in the apolar case, the nematic order is usually described by a tensorial order parameter $\mathbf{q}$ [4]. Here we are interested in the case of an apolar nematic but we will take advantage of the formulation in terms of a polarization field $\mathbf{p}$, which is possible because of the invariance of the equations to the $\mathbf{p} \rightarrow \mathbf{-p}$ change, and because we will deal with situations without topological defects [2].

Because of their complexity, it is very difficult to fully elucidate the dynamics of active matter in general, taking into account all the forces acting in them. However, the phenomenological approach of active gels theory, based on conservation laws and symmetries in the hydrodynamic limit, provides deep insights and a well-grounded guide to extract generic behaviour. In particular, one of the most important aspects when studying complex systems is the pursuit of universality, that is, of properties that may show some type of scale invariance that is insensitive to system-specific details, and may provide some type of classification of dynamical behaviour in a small number of universality classes, such as in equilibrium critical phenomena or turbulence in nonequilibrium systems.

Turbulence refers to fluid motion characterized by chaotic changes in pressure and velocity, and it is an important and longstanding unsolved problem in nonequilibrium and nonlinear physics. Classically, it appears in systems where the inertial forces prevail ($\mathrm{Re} \gg 1$) due to the advection term of the Navier-Stokes equation, and it was shown by Kolmogorov to present a power-law scaling spectrum $E(k) \sim k^{-5/3}$ being $k \rightarrow 0$ the wavenumber [5]. For active systems (and viscoelastic fluids) similar turbulence also appears at $\mathrm{Re} \ll 1$ where the viscous forces dominate. In fact, in a recent study addressing the simplest possible model of an active nematic fluid, a power-law turbulent spectrum $E(k) \sim k^{-1}$ has been observed [6]. Accordingly, such model has been proposed as the paradigm of a new universality class of turbulence.

In this context, our aim is to gain a deeper knowledge of the above minimal model and the mechanisms that characterize the transition to turbulence, starting by investigating the stationary states that emerge from the spontaneous flow instability [7] of an active fluid, and in particular their secondary instabilities as a possible route to turbulence, as a function of activity.

II. MINIMAL MODEL OF ACTIVE GEL

Following the active gels theory approach [3], using the Curie principle and the Onsager reciprocity relations, we can get the explicit hydrodynamic equations for an incompressible ($\partial_\alpha v_\alpha = 0$) one-component with $\mathrm{Re} = 0$ active nematic fluid in 2D (minimal model). The nematic fluid is confined in a square of side L with periodic boundary conditions, and has a shear viscosity η, a rotational viscosity γ and an activity $|\zeta \Delta\mu|$. An important simplification is to set the flow alignment coefficient $\nu = 0$. The polar nematic field is given by its unit director vector p_α chosen to be $p_x = \cos\theta$ and $p_y = \sin\theta$, such that it is kept unitary, and accordingly defects cannot be created.

*Electronic address: irinapijauma@gmail.com

Under these conditions the continuity equation for the conservation of linear momentum reads

$$\partial_\beta(\sigma_{\alpha\beta}+\sigma^a_{\alpha\beta})=\partial_\alpha P, \tag{1}$$

where P is the pressure, $\sigma_{\alpha\beta}=2\eta v_{\alpha\beta}-\zeta\Delta\mu q_{\alpha\beta}$ is the symmetric part of the stress tensor with $v_{\alpha\beta}=\frac{1}{2}(\partial_\alpha v_\beta+\partial_\beta v_\alpha)$ and $q_{\alpha\beta}=p_\alpha p_\beta-\frac{1}{2}p_\gamma p_\gamma\delta_{\alpha\beta}$ the symmetric parts of the strain rate tensor and the nematic order parameter tensor respectively, and $\sigma^a_{\alpha\beta}=\frac{1}{2}(p_\alpha h_\beta-p_\beta h_\alpha)$ is the antisymmetric part of the stress tensor with the molecular field $h_\alpha=K\nabla^2 p_\alpha$, being K the Frank constant [4]. Regarding the dynamics of the polarity field, given $\omega_{\alpha\beta}=\frac{1}{2}(\partial_\alpha v_\beta-\partial_\beta v_\alpha)$ the antisymmetric part of the strain rate tensor, we have

$$(\partial_t+v_\beta\partial_\beta)p_\alpha+\omega_{\alpha\beta}p_\beta=\frac{h_\alpha}{\gamma}. \tag{2}$$

In order to work with dimensionless variables, we scale lengths by L, time by $\gamma L^2/K$, pressure by $\eta K/\gamma L^2$ and stresses (polarity and molecular field) by K/L^2. The stream function ψ is introduced such that $v_x=\partial_y\psi$ and $v_y=-\partial_x\psi$, and let the dimensionless activity parameter (which expresses the ratio of active to elastic stresses) be

$$\mathcal{Z}\equiv\mathcal{S}\frac{|\zeta\Delta\mu|rL^2}{K}\equiv\mathcal{S}\frac{L^2}{l_c^2}, \tag{3}$$

where l_c is an intrinsic length of the problem, $r\equiv\gamma/\eta$ and $\mathcal{S}=-1(+1)$ for contractile (extensile) stresses. Also taking the curl of Eq.(1) we get

$$\nabla^4\psi+\frac{r}{2}\nabla^4\theta=\mathcal{Z}\Big(\frac{1}{2}(\partial_y^2-\partial_x^2)\sin 2\theta+\partial^2_{xy}\cos 2\theta\Big) \tag{4}$$

$$\partial_t\theta=\nabla^2\theta-\frac{1}{2}\nabla^2\psi+(\partial_x\psi)(\partial_y\theta)-(\partial_y\psi)(\partial_x\theta). \tag{5}$$

Slightly different equations are presented in [6] due to differences in the scaling, but all of them are equivalent. We will solve numerically these equations and focus in particular on the emergence of steady states.

A. Instability of the state with uniform orientation

An important result in [6] is that if a perturbation of wavevector $\vec{q}$, forming an angle ϕ with $\vec{p}_0=p_x$, is applied to the considered fluid, the most unstable mode of the perturbation (and so the dominant one) is that of the largest wavelength modulation that fits inside the system in the y-direction. Indeed, introducing the ansatz $\theta=\theta_0\exp\{i(q_x x+q_y y)+\Omega t\}$ and $\psi=\psi_0\exp\{i(q_x x+q_y y)+\Omega t\}$ in Eq.(4) and (5) and linearizing, it can be shown that the linear growth rate $\Omega(\vec{q})$ of the perturbation (amplitude $\propto e^{\Omega t}$) is given by

$$\Omega(q_x,q_y)=-\Big(1+\frac{r}{4}\Big)q^2+\frac{1}{2}\mathcal{Z}\cos 2\phi, \tag{6}$$

where $\cos 2\phi=(q_x^2-q_y^2)/(q_x^2+q_y^2)$. So the smaller is $|q|$ the higher the growth rate, defining unstable modes by the condition $\Omega>0$. Indeed, as a consequence of the linear analysis the most unstable mode will be that of minimum wavevector $|q_0|=2\pi/L$ and in the transversal (longitudinal) direction to $\vec{p}_0$, and so with $q_x=0$ ($q_y=0$) for contractile (extensile) stresses. The characteristic time of the problem is given by $t_c\sim 1/\Omega(0)$.

Stationary solutions for the polarity field ($\partial_t\theta=0$) can be found analytically for 1D perturbations (assuming $\partial_x=0\ \forall t$) [6], obtaining similar solutions to that of the pendulum equation. However, such solutions are not stable in 2D, so the existence and stability of steady states solutions in 2D must be explored numerically.

III. METHODS

A. Numerical algorithm

Fortran codes supplied by R. Alert are taken as the starting point and slightly adapted to each situation. An algorithm combining spectral methods and finite differences is used, in a way that simulations for the polarity field (as well as for the stream function) are performed in a lattice with n nodes in each direction, which represent real-space points or Fourier modes (so n must be a power of two). The larger n the better resolution, but the simulation time increases very strongly with it. Typically the initial condition for the angle field is chosen to be a small amplitude sinusoidal perturbation, $\theta(\vec{r},0)=\theta_0\sin(\vec{q}\cdot\vec{r})$, with amplitude $\theta_0=0.05\pi/2$ and $\vec{q}=2\pi/L(m_x,m_y)$ where $m_x,m_y\in\mathbb{Z}$. The final stationary state, if it exists, should not depend on the it.

The procedure then goes as following. First the field $\theta(\vec{r},t)$ and all the other nonlinear terms in Eq.(4) are Fourier transformed, so the stream function can be computed in the Fourier space taking into account that $\mathcal{F}[\partial^{(n)}f]=(iq)^n\tilde{f}$ (both $\mathcal{F}[\cdot]$ and $\tilde{\cdot}$ denoting the Fourier transform omitting the constants). This way

$$\tilde{\psi}_{\vec{q}}(t)=-\frac{r}{2}\tilde{\theta}_{\vec{q}}(t)+\frac{\mathcal{Z}}{q^4}\Big(\frac{q_x^2-q_y^2}{2}\mathcal{F}[\sin(2\theta)]_{\vec{q}}(t) -q_xq_y\mathcal{F}[\cos(2\theta)]_{\vec{q}}(t)\Big). \tag{7}$$

A prescription is needed in order to avoid the divergence due to the $\vec{q}=\vec{0}$ mode, so instead we divide by $q^4+\epsilon$ with $\epsilon=10^{-8}$. Then computing the inverse Fourier transform back to real space we get $\vec{\psi}(\vec{r},t)$, as well as the velocity field $\vec{v}(\vec{r},t)$ since $\vec{v}=\vec{\nabla}\times\vec{\psi}$. Finally, integrating the dynamics of the polarity field in Eq.(5) by the Euler's method, the solution for $\theta(\vec{r},t)$ is obtained. In principle it would be better to use an appropriate implicit algorithm such as the alternating-direction implicit (ADI) method, which would be faster and more stable, but such code is not yet fully developed.

All this procedure is repeated for a large number of time steps, summing an increment dt at each iteration and adding a little bit of noise (to ensure the robustness

of the dynamics) that could come in the real system from thermal or active fluctuations. Numerically, we must add a Gaussian white noise $\xi(\vec{r},t)$ such that $\langle\xi(\vec{r},t)\rangle = 0$ and $\langle\xi(\vec{r},t)\xi(\vec{r'},t')\rangle = 2D\delta(\vec{r}-\vec{r'})\delta(t-t')$ to the angle variable, being D the amplitude of the noise. Then, summing $\xi(\vec{r},t)$ to the right hand side of Eq.(5), it becomes a Langevin stochastic equation and is implemented within the Euler algorithm by adding the random contribution

$$\sqrt{\frac{2D\Delta t}{\Delta x\Delta y}}G(x,y),$$

where $G(x,y)$ are non correlated and independent Gaussian random numbers of unit variance. We will reach a stationary state when the results for the angle remain unchanged except for small fluctuations.

B. Simulation parameters

For all the simulations we have fixed $L = 1$ [dimensionless] and $\mathcal{S} = -1$ (we focus on contractile stresses as we expect similar qualitative results for extensile ones), and so we set $q_x = 0$ and $q_y = 2\pi/L = 2\pi$ in order to choose the most unstable mode of the perturbation (forming an angle $\phi = \pi/2$ with $\vec{p_0} = p_x$). We fix $r = 1$ and keep varying the activity parameter $\mathcal{Z} = -L^2/l_c^2$ (that is, varying the characteristic length l_c). The lattice we use has either $n = 128$ or 256 points, and only when the mosaic replicas (see below) are implemented we reach 512 (or 1024 for visualization). In order to ensure numerical stability, the higher n (and so the smaller the spacing), the smaller we have to make dt, so we use $dt = 10^{-5}, 10^{-6}$ or 10^{-7} [dimensionless] respectively. The number of steps we take depends a lot on the other variables, and the amplitude of the noise is taken to be $D = 5\cdot10^{-4}$ in the simulation units (results do not depend on it).

In order to find the stationary states and be able to study their stability, first we must know in which range of activity parameters they exist. Due to Eq.(6), for low activity parameters $\Omega < 0$ (in our case for $|\mathcal{Z}| < 10\pi^2$) and so the initially implemented perturbation will be stable because the amplitude will decrease (Fig.(1a,b)). But neither do we see any changes in the initial perturbation (except for some fluctuations) between $10\pi^2 < |\mathcal{Z}| < 150$, possibly because the evolution is very slow, and so we take 150 as the lower boundary. On the other hand, if we look into too high activities ($|\mathcal{Z}| > 2000$), the dynamics becomes turbulent, with the fields persistently varying in a chaotic way with no apparent convergence to a steady configuration (Fig.(1c,d)). Therefore, the chosen regime to study is $150 < |\mathcal{Z}| < 1500$. Between 1500 and 2000 (or possibly a bit higher) there could possibly still exist steady states, as we could suspect from some of the longest simulations that we did, but the limitation of simulation time did not yield a clear conclusion. They could either exist but not yet been reached, or the persistent dynamics be the signature of some chaotic attractor.

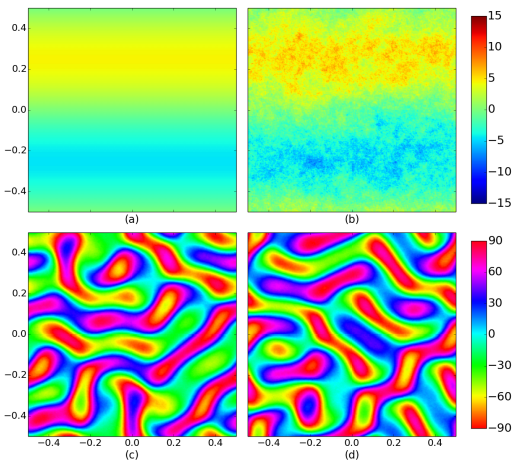

FIG. 1: Simulation of the polarity field in a lattice of 256 × 256 where color indicates the angle θ. We show the initial condition (a), the evolution after $t = 0.02 = t_c$ for $|\mathcal{Z}| = 100$ (b), the evolution after $t = 0.05 = 125t_c$ for $|\mathcal{Z}| = 5000$ (c) and the evolution after $t = 0.09 = 225t_c$ for $|\mathcal{Z}| = 5000$ (d). Clearly in (b) the angles are essentially the same as in the initial condition whereas in (c) and (d) results are statistically similar but have evolved a lot. Note that the color scales are different. From now on we will always plot the colorbar from -90° to 90° as we are considering a nematic fluid.

IV. RESULTS

A. Stationary states

In order to get the stationary states in a more efficient way, instead of starting for each $\mathcal{Z}$ from the explained initial condition, we follow a continuation method, namely, we start from the stationary state computed for the previous $\mathcal{Z}$. That is, first we reach the stationary state for the highest activity in our regime ($|\mathcal{Z}| = 1500$) starting from the initial perturbation, which is found after a simulation time of $t = 0.2 = 150t_c$. Then, using this one as the initial condition for $|\mathcal{Z}| = 1450$ we arrive more quickly to the steady state (gaining a factor of ten). We keep lowering the activity by steps of 50 until $|\mathcal{Z}| = 150$, and get, as a representative sample, the states in Fig.(2), which change continuously with the activity parameter. To describe how angles change, we have plotted in Fig.(3) the evolution with $|\mathcal{Z}|$ of three significant points in the simulations (a, b and c in Fig.(2) which are the relative extremes of the polarity field). Also, regarding the two elongated regions generated at low activities (I and II in Fig.(2)), we can plot the angle between them before the bottom one is split.

Moreover we have also carried out the simulations starting from different initial conditions, probing the basin of attraction of the states found from the continuation method. Of course we never get exactly the same configuration because the dynamics includes noise, so the location and orientation of the spots may vary

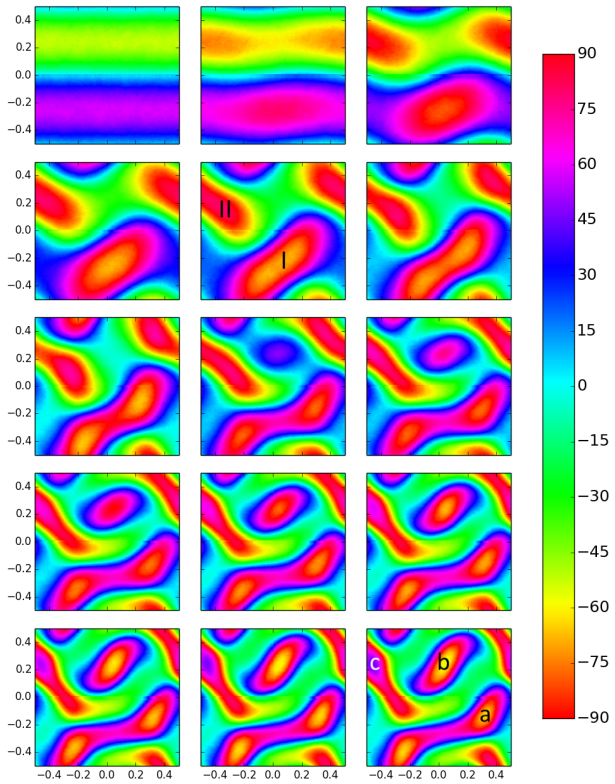

FIG. 2: Polarity field of the stationary states in a 256×256 lattice, for values of $|\mathcal{Z}| = 150$ (top left) to 1500 (bottom right) and increasing 100 at each figure (ordered by lines), except in the last step that increases from 1450 to 1500.

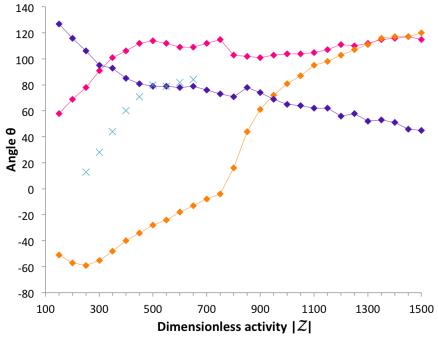

FIG. 3: Lines represent angles of the polarity field as a function of $|\mathcal{Z}|$ for the relative extremes. Taking the last (bottom right) figure in Fig.(2) as reference, the regions considered are: a (pink line), b (orange line) and c (purple line). In order to make the plots continuous (as is the angle) we use that $\theta = \theta \pm 180$ (nematic), and so for example both the orange and the purple line start in a very close angle. The pink and the purple evolve similarly but in an opposed way. Crosses represent the angle between I and II in Fig.(2), seeing that then I is divided at $\sim 80° - 85°$.

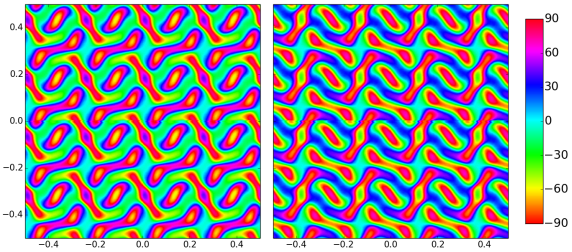

FIG. 4: Polarity field of the stationary states obtained for $|\mathcal{Z}| = 1500$ with two different initial conditions: starting from the initial perturbation (left) and starting from $|\mathcal{Z}| = 150$ and increasing 50 at each step (right). It is plotted in a 1024×1024 lattice for a better visualization, but taking into account just one cell, both patterns are the same with a $x \to -x$, $y \to y$ and $\theta \to -\theta$ transformation (although for angles in between -90° and 90° the mirror symmetry would be $\pm\theta \to \pm 180 \mp \theta$, 180° must be subtracted or summed again because of the nematic condition and so we get the opposed angle).

due to continuous symmetries of the dynamics. For most values of $|\mathcal{Z}|$ we have explicitly checked that the steady state reached from the initial instability is equivalent to the one obtained from the continuation method described above, thus confirming a large basin of attraction of such steady states, possibly including the whole space of initial conditions. These tests also show that the steady states may have some degeneracy due to discrete symmetries, such in the case shown in Fig.(4).

B. Stability

From what we have pointed out in section II A, if we have a system in a stationary state and increase its dimensions, we can expect it to evolve as then a larger wavelength perturbation fits inside the system (unstable stationary state). In this way, by replicating the states obtained in Fig.(2) and so generating a mosaic of larger dimensions, we can effectively investigate the stability of periodic patterns to perturbations of wavelength larger than the period of the pattern.

As $L = 1$ is always fixed in our simulation, duplicating n (simulations in a 512×512 lattice) is equivalent to dividing the characteristic length $l_c' = l_c/2$, so in order to have the same activity parameter each time we must set $|\mathcal{Z}|' = 4|\mathcal{Z}|$. Then, from the mosaic of stationary states we introduce a perturbation of wavevector $|q| = 2\pi$ both in x and y (breaking the periodicity of the small system but not of the big one) and let it evolve. This procedure implements a period-doubling perturbation. In some cases ($|\mathcal{Z}| = 500$ and 600) we could not elucidate whether the system returned to the stationary state or not, because either it takes too long to return there, or some attractors states exist in which the system stays for a long time. Thus, we started from their stationary states obtained with $n = 128$ (instead of 256) and duplicate those (256×256 lattice). Some representative results are the ones in Fig.(5). It is clear then that for low activities (until $|\mathcal{Z}| = 500$) the mosaics are

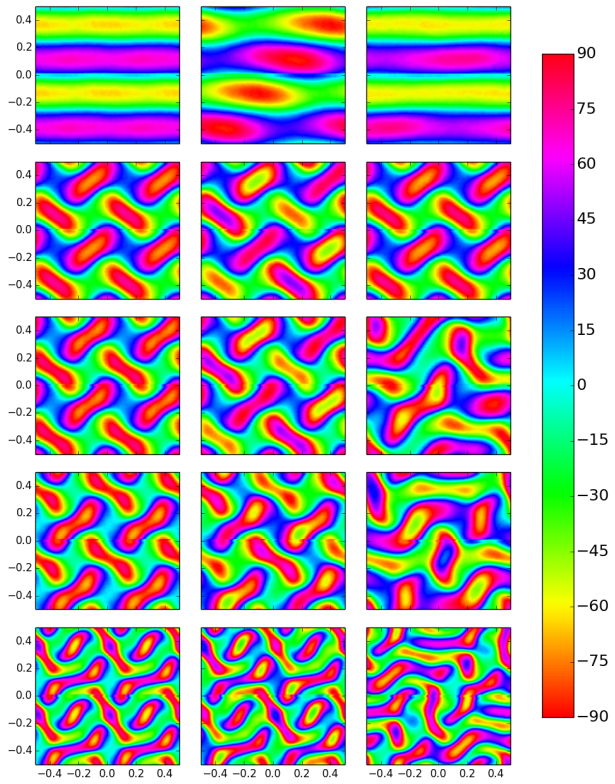

FIG. 5: Polarity field for $|\mathcal{Z}| = 200, 500, 600, 700$ and 1500 respectively in each row. In a fixed row, polarity field of the steady state for the smaller system (first column), after the perturbation (second column) and after a significant time simulation (third column), always bigger than t_c.

stable under period-doubling perturbations, as they return to the unperturbed mosaic, whereas for higher ones (from $|\mathcal{Z}| = 600$) they evolve into persistent, apparently turbulent dynamics. These preliminary results should be completed with longer time simulations, and perturbations of longer wavelength.

V. DISCUSSION AND CONCLUSIONS

- We have found explicitly a series of asymptotic steady states as a function of activity, which exist at least up to $|\mathcal{Z}| = 1500$, showing their qualitative evolution for increasing activity, from stripes, to undulated stripes, to rhombic arrangements of elongated spots, reaching an angle of $\sim 85°$ (at $|\mathcal{Z}| = 650$), that then split into more complex structures. We have also characterized quantitatively the polarization angles at the their local extrema.
- We have shown that the basin of attraction of those steady state is large, including the neighborhood of the homogeneous unstable states.
- We have found that for low activities ($|\mathcal{Z}| \leq 500$) the steady states are stable under period-doubling perturbations, since perturbed mosaic replicas return to them, whereas for higher activities they evolve to states with apparently persistent dynamics.
- The study confirms a long-wavelength instability of the periodic patterns obtained, implying that for sufficiently large activity (or sufficiently large systems) the system evolves to chaotic dynamics, possibly defining the universality class of active turbulence.

The above results contribute to our understanding of the transition to turbulence in active systems. Further investigation should explore larger systems and longer times, to complete the analysis and to pursue a quantitative characterization of the chaotic dynamics, in particular for weakly turbulent regimes. The long-wavelength instability of periodic states should be explored more rigorously diagonalizing numerically the linear dynamics around the nonlinear steady states. Finally, the extension to finite flow alignment coefficient would be required to justify the claims of universality.

Acknowledgments

I am sincerely grateful to my advisor Prof. Jaume Casademunt, for your patience, guidance, knowledge and motivation throughout all the project, and for having introduced me to this amazing field as Biophysics is. Also to Dr. Ricard Alert, for the codes and availability in helping me. And finally thank you to my family, friends, and above all to Quim, for your unconditional support during all these years.

[1] F. Schweitzer, *Brownian Agents and Active Particles: Collective Dynamics in the Natural and Social Sciences*, (Springer, Berlin, 2003).
[2] M.C. Marchetti, et al., "Hydrodynamics of soft active matter". Rev. Mod. Phys. **85**, 1143 (2013).
[3] J. Prost, F. Jülicher, and J.F. Joanny, "Active gel physics". Nat. Phys. **11**, 111-117 (2015).
[4] P.G. de Gennes and J. Prost, *The Physics of Liquid Crystals*, (Clarendon Press, Oxford, 1993).
[5] A.N. Kolmogorov (translation by V. Levin), "The local structure of turbulence in incompressible viscous fluid for very large Reynolds numbers". Proceedings of the Royal Society A. **434**, 9-13 (1991).
[6] J. Casademunt, R. Alert, and J.F. Joanny, "Universal scaling of defect-free active turbulence" (unpublished).
[7] R. Voituriez, J.F. Joanny, and J. Prost, "Spontaneous flow transition in active polar gels". Europhys. Lett. **70**, 404-410 (2005).